

Pole trajectories of the $\Lambda(1405)$ towards the $SU(3)$ limit

QCHSC2024

R. Molina (Raquel.Molina@ific.uv.es)

Zejian Zhuang, Li-Sheng Geng, Jun-Xu Lu

arXiv: 2405.07686





Introduction: Two pole structures

Meson-Baryon scattering

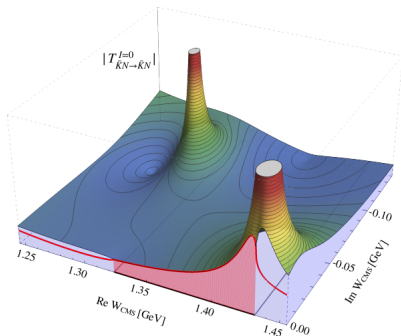
The $\Lambda(1405)$ (finite volume)

Conclusions

Two pole structures



$\Lambda(1405)$



2nd Riemann Sheet

$$\frac{1}{\sqrt{s} - M_R + i\Gamma/2}$$

$$\Gamma/2 = \beta p$$

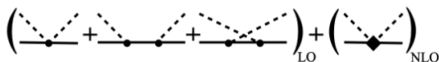
$$\sqrt{s} = a + ib$$

$$\frac{1}{a - M_R + ib + i\beta p}$$

Change $p \rightarrow -p$
gives a solution

Figure taken from Review of the $\Lambda(1405)$, Mai (2020)

$\pi\Sigma, \bar{K}N$



Two pole structures



- ▶ At LO the interaction is diagonal $V_{\alpha\beta} = -\frac{1}{4f^2} C_{\alpha\beta} (k^0 + k'^0)$.

$$V_{\alpha\beta} = \text{diag}(6, 3, 3, 0, 0, -2) \quad \alpha, \beta = 1, 8, 8', 10, \bar{10}, 27 \quad (1)$$

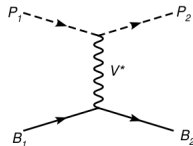
- ▶ At NLO the accidental symmetry of the two octets is slightly broken ($\Delta M_8 \simeq 15$ MeV) [Guo, Kamiya, Mai, Meissner PLB23](#)
- ▶ The most important features obtained at LO remain at NNLO.
(LO) [Jido, Oller, Oset, Ramos, Meissner NPA03](#)
(NNLO) [Lu, Geng, Doering, Mai PRL23](#)

$$(LO) \quad \sqrt{s_0} : 1390 - i66, \quad 1426 - i16$$

$$(NNLO) \quad \sqrt{s_0} : 1392 \pm 8 - i(100 \pm 15), \quad 1425 \pm 1 - i(13 \pm 4)$$

**Weinberg-Tomozawa
dominates**

BaSc, PRL132 (2024)





- ▶ Chiral Lagrangians for the Meson-Baryon interaction:
Pich, RPP95; Ecker, PPNP94, Bernard, Kaiser, Meissner, IJNPE95;
Meissner, RPP93

$$\mathcal{L} = \mathcal{L}_\phi + \mathcal{L}_{\phi B}, \quad (2)$$

Lowest order:

$$\mathcal{L}_{\phi B}^{(1)} = i\langle \bar{B}\gamma_\mu [D^\mu, B] \rangle - M_0\langle \bar{B}B \rangle - \frac{1}{2}D\langle \bar{B}\gamma_\mu\gamma_5\{u^\mu, B\} \rangle - \frac{1}{2}F\langle \bar{B}\gamma_\mu\gamma_5[u^\mu, B] \rangle$$

Next-to-leading order

$$\begin{aligned} \mathcal{L}_{\phi B}^{(2)} = & b_D\langle \bar{B}\{\chi_+, B\} \rangle + b_F\langle \bar{B}[\chi_+, B] \rangle + b_0\langle \bar{B}B \rangle\langle \chi_+ \rangle \\ & + d_1\langle \bar{B}\{u_\mu, [u^\mu, B]\} \rangle + d_2\langle \bar{B}[u_\mu, [u^\mu, B]] \rangle \\ & + d_3\langle \bar{B}u_\mu \rangle\langle u^\mu B \rangle + d_4\langle \bar{B}B \rangle\langle u^\mu u_\mu \rangle, \end{aligned} \quad (3)$$



Channels for $l = 0, S = -1$: $\pi\Sigma, \bar{K}N, \eta\Lambda, K\Xi$

- ▶ Weinberg-Tomozawa+NLO:

$$V_{ij} = -\frac{N_i N_j}{4f^2} \left[C_{ij} (2\sqrt{s} - M_i - M_j) - 4(D_{ij} - 2k_\mu k'^\mu L_{ij}) \right] \quad (4)$$

$$N_i = \sqrt{(M_i + E_i)/2M_i}$$

M_i, E_i baryon mass and energy of the channel i

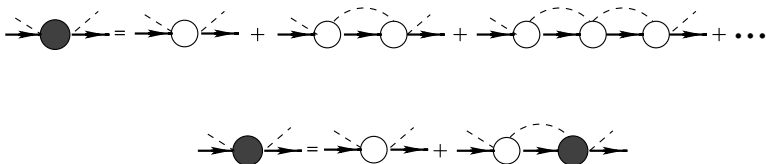


Figure: Diagrammatic solution of the Bethe-Salpeter equation.



Scattering amplitude in Bethe-Salpeter:

$$T^{-1} = V_0^{-1} - G. \quad (5)$$

where $V_0 \equiv V_{(L=0)}$ is the s -wave projection.

$$G_j = 2iM_j \int \frac{d^4q}{(2\pi)^4} \frac{1}{q^2 - m_j^2 + i\epsilon} \frac{1}{(P - q)^2 - M_j^2 + i\epsilon}. \quad (6)$$

The loop function can be evaluated in the Dimensional Regularization (DR) or cutoff scheme (q_{\max}). Oller, Meissner, PLB01:

$$G_i(s) = \frac{2M_i}{16\pi^2} \left\{ a_i(\mu) + \ln \frac{M_i^2}{\mu^2} + \frac{m_i^2 - M_i^2 + s}{2W^2} \ln \frac{m_i^2}{M_i^2} \right. \\ \left. + \frac{\bar{q}_i}{\sqrt{s}} \left[\ln(s - (M_i^2 - m_i^2) + 2\bar{q}_i\sqrt{s}) + \ln(s + (M_i^2 - m_i^2) + 2\bar{q}_i\sqrt{s}) \right. \right. \\ \left. \left. - \ln(-s + (M_i^2 - m_i^2) + 2\bar{q}_i\sqrt{s}) - \ln(-s - (M_i^2 - m_i^2) + 2\bar{q}_i\sqrt{s}) \right] \right\},$$



By comparing these two formulas, Oller, PPNP20:

$$a(\mu) = -\frac{2}{m+M} \left[m \log\left(1 + \sqrt{1 + \frac{m^2}{q_{\max}^2}}\right) + M \log\left(1 + \sqrt{1 + \frac{M^2}{q_{\max}^2}}\right) \right] + 2 \log\left(\frac{\mu}{q_{\max}}\right). \quad (7)$$

with $\mu = 630$ MeV (Oset, Ramos, NPA98). Analytical continuation of G :

$$G_i^{\prime\prime}(s) = G_i(s) + i \frac{2M_i q_{\text{cm}}}{4\pi\sqrt{s}}, \quad \text{Im}q_{\text{cm}} > 0. \quad (8)$$

Near to the resonance region:

$$T_{ij} \simeq \frac{g_i g_j}{\sqrt{s} - \sqrt{s_0}}, \quad (9)$$

g_i coupling to the channel i . The phase shift is:

$$p \cot \delta_j = -\frac{8\pi E}{2M_j} (T_{jj})^{-1} + i p_j, \quad (10)$$



- ▶ Input: RQCD, JHEP23. Chiral trajectories $\text{Tr}[M] = C$, $m_s = m_{s,\text{phy}}$, and $m_s = m_l$, $l = u, d$
- ▶ CoBChPT. J. Martín-Camalich, L. S. Geng. M. J. Vicente-Vacas, JHEP05(2023)

$$m_B = m_0 + m_B^{(2)} + m_B^{(3)}, \quad (11)$$

$$m_B^{(2)} = \sum_{\phi=\pi,K} -\xi_{B,\phi}^{(a)} m_\phi^2, \quad (12)$$

$$m_B^{(3)} = \sum_{\phi=\pi,K,\eta} \frac{1}{(4\pi f_\phi)^2} \xi_{B,\phi}^{(b)} H_B^{(b)}(m_\phi), \quad (13)$$

Polynomial+loop. D, F (nuclear beta decay, Borasoy, PRD98)

$$D = 0.80, F = 0.46. \quad (14)$$



	m_0 [MeV]	b_0 [GeV ⁻¹]	b_D [GeV ⁻¹]	b_F [GeV ⁻¹]
This work	805(40)(40)	-0.665(40)(28)	0.062(26)(8)	-0.354(18)(9)
RQCD23	821 ⁽⁷¹⁾ ₍₅₃₎	-0.739 ⁽⁷⁰⁾ ₍₈₄₎	0.056 ⁽⁴³⁾ ₍₃₉₎	-0.44 ⁽⁴⁰⁾ ₍₂₆₎

- Covariance matrix obtained in the LQCD simulation is taken into account

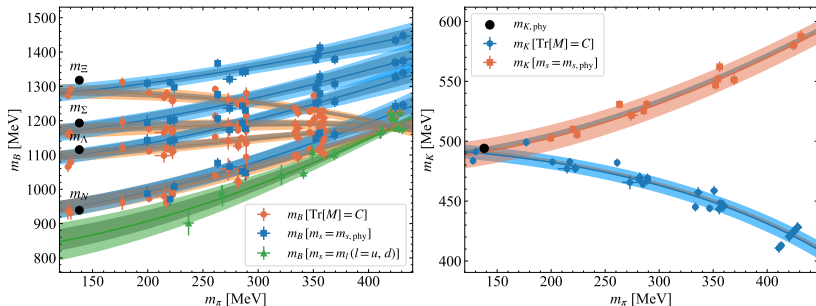
$$\chi^2 = \Delta E^T C_E^{-1} \Delta E \quad (15)$$

b_i are related to the splitting of the octet baryon masses and pion-nucleon sigma term (Gasser,PLB91). Chiral trajectories:

$$m_{0K}^2 = B_0 C - \frac{m_{0\pi}^2}{2}, \quad \text{Tr}[M] = C$$

$$m_{0K}^2 = B_0 m_{s,\text{ph}} + \frac{m_{0\pi}^2}{2}, \quad m_s = m_{s,\text{ph}} \quad (16)$$

Figure: Baryon masses over the different chiral trajectories.



For the masses and decay constants of pseudoscalar mesons, we take the LECs L_i^r 's from a global fit that includes also the data of the CLS ensembles, Molina and Ruiz de Elvira, JHEP20



Scattering amplitude in the finite volume:

$$\tilde{T}^{-1} = V_0^{-1} - \tilde{G}, \quad (17)$$

The loop function \tilde{G} in the finite volume can be calculated in DR,

$$\tilde{G}(P^0, \vec{P}) = G^{DR}(P^0, \vec{P}) + \lim_{q_{\max} \rightarrow \infty} \Delta G(P_0, \vec{P}, q_{\max}), \quad (18)$$

G^{DR} : loop function in the infinite volume, $\Delta G = \tilde{G}^{co} - G^{co}$.

Loop function evaluated with cutoff in the finite volume:

$$\tilde{G}^{co} = \frac{2M}{L^3} \sum_n^{q_{\max}} \frac{E}{P_0} I(q^*), \quad (19)$$

q^* : center-of-mass (CM) momentum, $\vec{q}_1^* + \vec{q}_2^* = 0$, $P^\mu = q_1^\mu + q_2^\mu$,
 $s = P_0^2 - \vec{P}^2$.



The function $I(q)$ reads,

$$I(\vec{q}) = \frac{\omega_1(q) + \omega_2(q)}{2\omega_1(q)\omega_2(q) [P_0^2 - (\omega_1(q) + \omega_2(q))^2 + i\epsilon]}, \quad (20)$$

with $\omega_i = \sqrt{q^2 + m_i^2}$, and $q = |\vec{q}|$.

Neglecting effects from higher partial waves, the energy levels are given solely by,

$$\det[I - V_0 \tilde{G}] = 0. \quad (21)$$

We take into account the covariance matrix of the energy levels from the LQCD simulation.

$$\chi^2 = \Delta E^T C_E^{-1} \Delta E \quad (22)$$

Energy Levels for $\bar{K}N - \pi\Sigma$ scattering ($I = 0$)

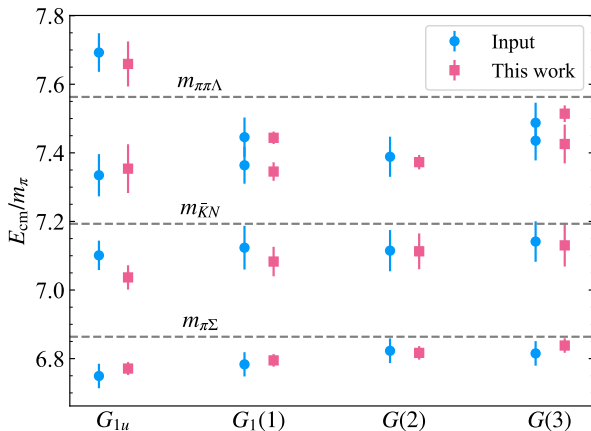


Figure: Finite-volume spectrum (circle points) in the center-of-mass frame used as input to constrain the free parameters of the chiral Lagrangian up to NLO. Input: J. Bulava, BaSc, PRD24, PRL24.



Table: Results for the LECs and cutoff $q_{\max} = 710(39)(40)$ MeV obtained in the fit. LECs in GeV^{-1} .

d_1	d_2	d_3	d_4
-0.36(20)(20)	0.02(1)(1)	-0.14(10)(10)	-0.58(20)(20)

We obtain $a \simeq -2$ (natural value, Oller, Meissner, PLB01).

$$a_{\pi\Sigma} = -2.30, a_{\bar{K}N} = -2.10 \quad m_\pi = 200 \text{ MeV}$$

$$a_{\bar{K}N} = -2.33, a_{\pi\Sigma} = -2.07 \quad m_\pi = 138 \text{ MeV}$$

$$a_{\bar{K}N} = a_{\pi\Sigma} = -2.25 \quad m_\pi = 423 \text{ MeV (SU3 limit)}$$

q_{\max} similar to Oset, Ramos, NPA98 (630 MeV). Only LO,
 $q_{\max}^{\text{LO}} = 632 \pm 90$ MeV. **Guo, Kamiya, Mai, Meissner PLB23, $a_{SU(3)} = -0.92$.**



Table: Pole positions of the $\Lambda(1405)$ for $m_\pi = 138$ and 200 MeV.

m_π [MeV]	138		200	
	z_1	z_2	z_1	z_2
Pole [MeV]	[1365(4)(10), 105(3)(7)]	[1420(4)(5), 10(3)(6)]	1380(7)(10)	[1454(5)(7), 13(4)(6)]
$ g_{\pi\Sigma} $	2.8(1)(3)	1.0(2)(4)	3.8(9)(10)	1.3(2)(4)
$ g_{\bar{K}N} $	1.8(3)(6)	3.0(2)(4)	1.7(3)(3)	3.0(2)(4)
$ \frac{g_{\pi\Sigma}}{g_{\bar{K}N}} $	1.6(9)(3)	0.3(1)(1)	2.4(8)(10)	0.4(1)(1)

Pole positions and couplings in LQCD ($m_\pi \simeq 200$ MeV):

$z_1 = 1392(9)(2)(16)$ MeV, $z_2 = 1455(13)(2)(17) - i11.5(4.4)(4)(0.1)$

Ratios of the couplings:

$$\left| \frac{c_{\pi\Sigma}^{(1)}}{c_{\bar{K}N}^{(1)}} \right| = 1.9(4)_{\text{st}}(6)_{\text{md}},$$

$$\left| \frac{c_{\pi\Sigma}^{(2)}}{c_{\bar{K}N}^{(2)}} \right| = 0.53(9)_{\text{st}}(10)_{\text{md}}.$$

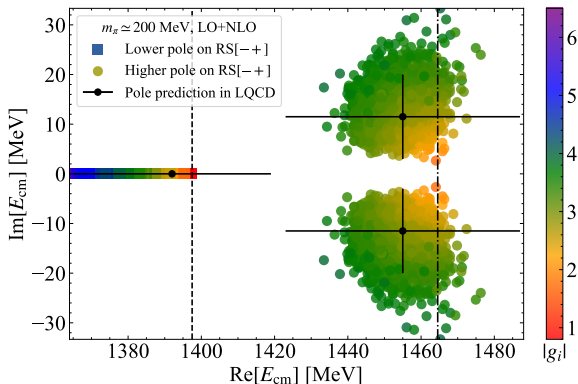


Figure: Pole positions of the $\Lambda(1405)$ for $m_\pi \simeq 200$ MeV at $1\text{-}\sigma$ (68%) confidence level. The error bars in black denote the LQCD results. The dashed line represents the $\pi\Sigma$ threshold and the dot-dashed line is the $\bar{K}N$ threshold.

Phase shifts: Comparison with LQCD

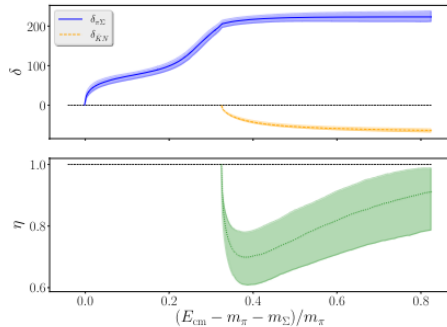
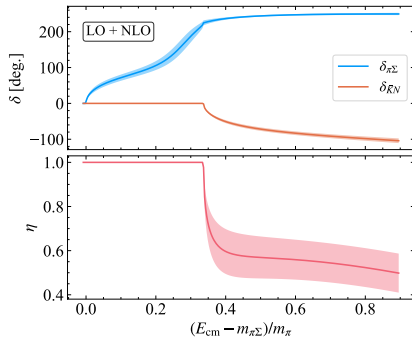
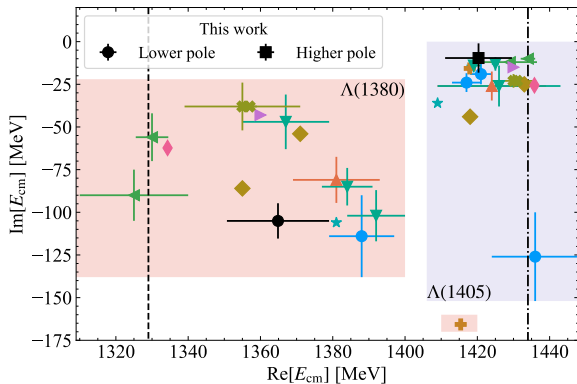


Figure: Comparison with the result from LQCD, BaSC Collaboration (right).

Comparison with experiment



NLO: ● Guo12 ▲ Ikeda12 ◀ Mai14 ▶ Sadasivan2018 ◆ Cieply11 ★ Shevchenko11 ◆ Haidenbauer10 ✕ Guo23 ★ Sadasivan:22
NNLO: ▼ Lu22

Figure: Pole positions of the two $\Lambda(1405)$ in comparison with other studies.

Comparison with experiment

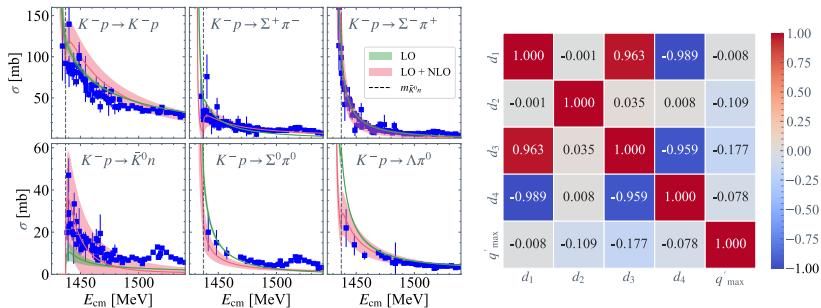


Figure: Comparison of the cross sections predicted by the model and the experimental data. The error bands of the cross sections are constrained by the correlation matrix of the fit to the LQCD energy levels.



$$a_{\bar{K}N} = a_{\pi\Sigma} = -2.25$$

Table: Pole positions for $m_\pi = 423$ MeV up to NLO.

m_π [MeV]	423		
	z_1	z_2	z_3
Pole [MeV]	1583(5)(1)	1585(8)(2)	1601(12)(2)
$ g_{\pi\Sigma} $	0.9(4)(8)	1.4(4)(6)	1.4(3)(1)
$ g_{\bar{K}N} $	1.1(4)(6)	2.1(5)(2)	0.6(6)(2)
$\left \frac{g_{\pi\Sigma}}{g_{\bar{K}N}} \right $	0.8(5)(9)	0.7(5)(2)	2.3(10)(10)

LO: $E^{(1)} = 1549(7)$ MeV, $E^{(8)} = E^{(8')} = 1602(4)$ MeV. At NLO, i.e., $\Delta E = E^{(8')} - E^{(8)} \approx 16$ MeV. 140 MeV difference with Guo, Kamiya, Mai, Meissner PLB23: 1704 and 1788 MeV, $\Delta E_8 = 15$ MeV ($m_\pi = 659.4$ MeV).

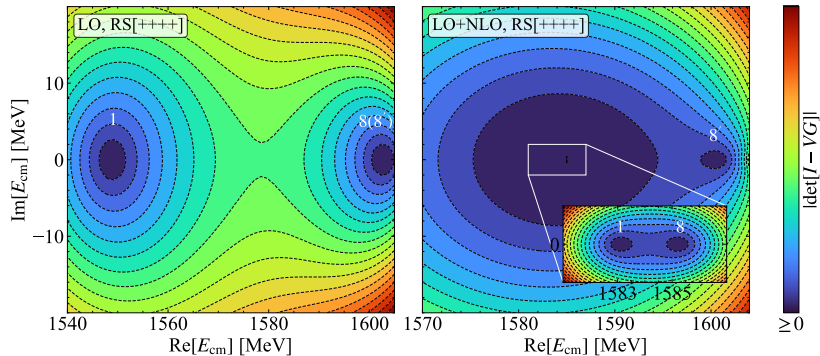


Figure: The contour of $|\det[I - VG]|$ in the SU(3) limit. The blue contours represent the pole positions of the four-coupled-channel scattering amplitude on the physical sheet.

Trajectories of the poles towards SU(3)

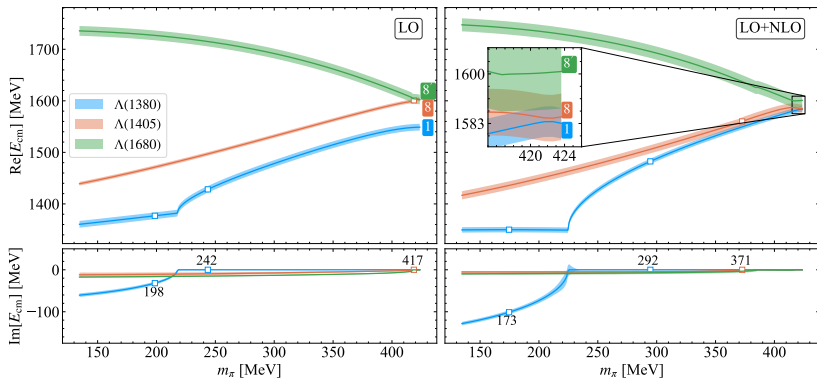


Figure: The trajectories of the three poles at LO (left panel) and up to NLO (right panel) for the $\Lambda(1405)$ and $\Lambda(1680)$. Lines in black are thresholds.

Trajectories of the poles towards SU(3)

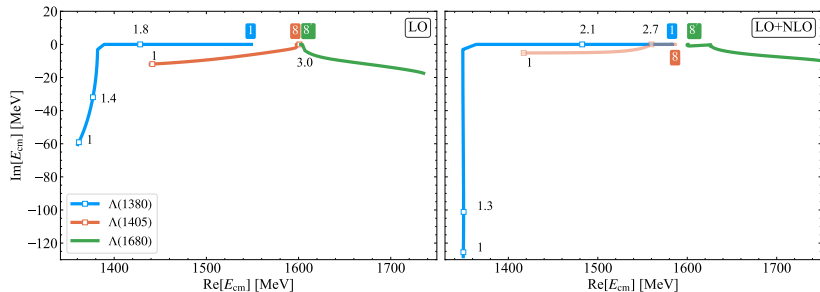


Figure: Motion of the poles from the SU(3) limit, where $r = m_{\pi}/m_{\pi,\text{phy}} = 3.07$, to the physical value, with $r = 1$. The numbers in the figure are the values of the ratios r .

We do not observe that the trajectories exchange when the NLO is included (Guo, Kamiya, Mai, Meissner PLB23). Result in qualitative agreement with Jido, Oset, Ramos, Meissner, NPA03, and Bruns, Cieply, NPA22.



- ▶ Finite volume is an useful tool. We have conducted a precise study for the $\Lambda(1405)$ quark mass dependence and the two-pole trajectories to the SU(3) limit.
- ▶ Our result supports the two pole structure of the $\Lambda(1405)$
- ▶ We find also that this LQCD data analysis is consistent with experimental data.